Vilniaus universiteto

Fizikos fakulteto

Lazerinių tyrimų centras

Mindaugas Česnulis

PAVIRŠIAUS DRĖKINIMO KONTROLĖ PTFE MEDŽIAGOSE FEMTOSEKUNDINIAIS LAZERIO IMPULSAIS

Bakalauro studijų baigiamasis darbas

Šviesos technologijų studijų programa

Studentas	Mindaugas Česnulis
Leista gintis	2023 – 01 – 11
Darbo vadovas	Doc. Domas Paipulas
Centro direktorius	Prof. Aidas Matijošius

Vilnius 2023

Vilnius university

Faculty of physics

Laser research center

Mindaugas Česnulis

WETTABILITY CONTROL OF PTFE SURFACES WITH FEMTOSECOND LASER PULSES

Final thesis of bachelor studies

Light Engineering study programme

Student	Mindaugas Česnulis
Allowed to defend	2023 – 01 – 11
Supervisor	Doc. Domas Paipulas
Director of center	Prof. Aidas Matijošius

Vilnius 2023

Table of Contents

Introduction

Today modern technologies allow to change various properties of the materials by providing them uniqueness. Usually as the inspiration source, scientists try to mimic nature, for example, lizard skin on steel to change its wettability.[1] To achieve this, physical, chemical and optical properties of matter can be varied by means of light. Extraordinary light produced by lasers can be used to process variety of materials including a diamond – one of the hardiest substance – in a contactless way, meaning that neither wear of tools nor mechanical friction is present during the process.[2] Laser micromachining is a subtractive fabrication technique, which uses focused laser beam to modify surface or volume of matter. It is a versatile and attractive processing method with wide tunability of fabrication parameters including wavelength, pulse energy, polarization, pulse repetition rate and speed of machining depending on specific application. A special niche is occupied by femtosecond laser micromachining, which possesses precision in the scale of micrometers and can be applied for different materials – metals, polymers, semiconductors, crystals, glasses, etc. In addition to this, hybrid fs micro processing is possible even in transparent materials by means of nonlinear optical phenomena.[3] This enables to alter properties of well-known polymers, for instance, polytetrafluoroethylene (PTFE), which are hard to process in traditional ways. In this work, femtosecond laser microfabrication is exploited to produce water repellent surfaces on PTFE polymer with the aim to investigate different fabrication parameters impact on its wettability control.

The tasks of this work:

1. To get acquainted with current situation on wettability control of PTFE surfaces using laser micromachining.
2. To compare impact of different laser wavelengths on textured PTFE surface properties.
3. To find optimal fabrication parameters to achieve highest water contact angle for laser-patterned PTFE surface.

1. Literature overview

1.1. Surface wettability

Wetting is an ability of liquid to spread throughout the surface of the material. Depending on surface parameters and liquid, spilled fluid can easily cover the surface or shrink to spherical and homogenous drops. Quantitively, wettability is described by the Contact Angle (CA), which is the angle between two tangent lines of the air-liquid and liquid-solid interfaces of the drop resting on flat surface.[4] Depending on value of the contact angle, surfaces are classified into four wetting regimes: superhydrophilic, hydrophilic, hydrophobic and superhydrophobic (SHP), where CA increases respectively as seen in Figure 1. Another parameter for quantitative measure of wettability is surface sliding angle, which is the critical angle of surface to horizontal reference line when a drop starts to roll.

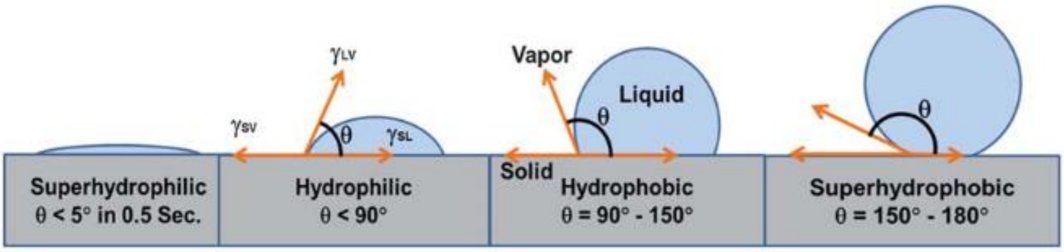

Figure 1. Types of wetting behavior on the surface according to contact angle.[5]

One of the parameters influencing surface wettability is surface free energy (SFE).[4] Chemically, it can be understood as the amount of chemical potential energy difference between surface and bulk atoms, that surface atoms attempt to minimize by attracting or bonding other atoms or molecules from outside. SFE is proportional to unpaired dangling bonds of the material surface atoms or molecules. Inside volume of the solid body, the chemical bonds are completely tightly connected and potential energy is minimal, whereas at the periphery, surface atoms do not form all the bonds and value of their potential energy is greater than bulk atoms.[6] Surface atoms have dangling bonds, which tend to minimize the energy by attracting the matter. For instance, after modifying steel with laser irradiation to create SHP surface, initially surface possesses hydrophilic behavior and after exposure to ambient environment its contact angle gradually increases.[7] It can be explained by surface chemistry modification with (in)organic constituents from air, which implies high surface energy immediately after fabrication, many dangling bonds and energy reduction by chemical reactions afterwards. It was even demonstrated that additional textured metal surface heating up to 250 °C catalyses chemical reactions and triggers fast wetting regime transition from hydrophilic to superhydrophobic.[8]

Surface morphology or roughness is another factor, which influences wettability of the surface.[4] According to heterogenous Cassie–Baxter wetting model, liquid drop on the surface stands on small surface features and protrusions caused by overall surface roughness (Fig. 2c).[9] The space between drop, supported by surface protrusions, and solid body is filled with air, thus liquid is in contact only with the small area of surface features and hangs on air pillow, thus can easily roll off. The contact angle in this case can be expressed by Cassie–Baxter equation: [9]

$$\cos(\theta_{CB}) = f\,(\cos(\theta) + 1) - 1\ , \tag{1}$$

where θ_{CB} is contact angle for Cassie-Baxter wetting model on rough surface, θ - contact angle on flat matter and f – fraction of liquid in contact with the solid material. In this case, drop forms spherical shape supported by liquid surface tension forces itself and can be a bit distorted by a gravity force. Morphology or surface texture is measured by surface roughness (R_a), which is average heights deviation from the reference flat line of the surface profile.

1.2. Basic wetting theories

Experiments on contact angle measurements of various liquids on solids have shown tendencies regarding specific material parameters. In 1805 Thomas Young presented mathematical relation between contact angle and surface tensions of gas, solid and liquid interfaces.[10] This is valid only for completely flat, chemically inert and uniform surfaces and expressed as contact angle at equilibrium conditions (θ_Y):

$$\cos(\theta_Y) = \frac{(\gamma_{SG} - \gamma_{SL})}{\gamma_{LG}}\ , \tag{2}$$

where γ is surface tension force of solid (S), liquid (L) and gas (G) interfaces (Fig. 2a). However, in nature none of the surfaces are ideally flat as described using the equation above and grooves, protrusions must be included. For rough surface Wenzel proposed equation relating Young's CA and surface roughness:

$$\cos(\theta_W) = R_a \cos(\theta_Y)\ , \tag{3}$$

here θ_W – Wenzel or apparent CA, R_a – surface roughness and θ_Y – CA of Young's model. In this model water fills the gaps and holes of material surface if surface roughness value $r \leq 1.7$ μm (Fig. 2b).[4] If roughness is greater, air is able to ingress between the liquid-solid interface forming a gap and the wetting regime is described according to equation (1) conforming Cassie–Baxter model as described in 1.1 section. In this work Cassie–Baxter model is essential at explaining wetting of polymer with artificially induced surface roughness.

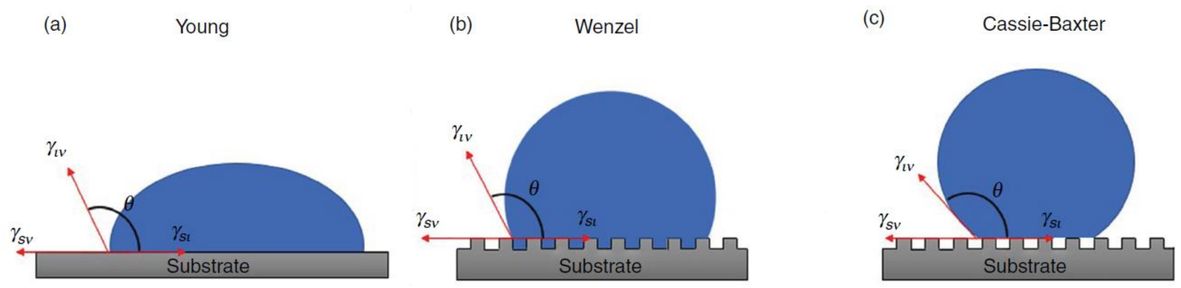

Figure 2. Graphical summary of three basic wetting models: (a) Thomas Young (b) Wenzel (c) Cassie-Baxter. [4]

1.3. Superhydrophobicity

Hydrophobicity refers to the property of the surface to repel water and possess low CA regime when a drop rests on it. Particularly superhydrophobic surfaces stand out due to its anti-bacterial, anti-icing and self-cleaning features.[11] The latter can be observed, when a water drop with SHP CA rolls off the surface capturing any dust present on its trajectory. Due to low SFE of material, dust sticks to a water drop and is being removed together with a drop showing surface self-cleaning capabilities. Another property of superhydrophobic surfaces can be anti-bacterial behaviour. On completely dry surface, population of bacteria is unable to attach and proliferate, thus scientists try to mimic the properties of such surfaces to achieve the least bacteria adhesion for applications in medicine.[12]

The most significant example of natural SHP surface possessing above mentioned properties is lotus leaf. It has hierarchical structures of branched micro papillae (in range of few μm) with nano features (hundreds of nm) overlayed by organic epicuticular vaxes, [4] as can be seen in Figure 3.

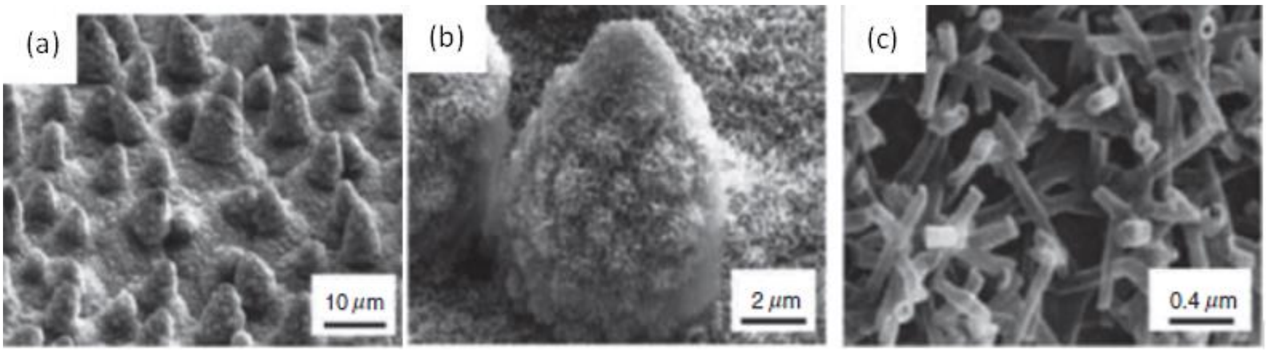

Figure 3. Lotus leaf surface SEM micrographs (a) and (b) of randomly distributed micro pillars and (c) nano-scale branches on them.[13]

The synergy of hierarchical structures along with the waxes shows water CA of about 164° and sliding angle below 3° on the leaf altogether with self-cleaning and anti-pathogenic capabilities.[6,12,14]

Due to these properties lotus effect is mostly considered as a synonym for self-cleaning properties originated from SHP leaves of nelumbo (lotus) flower.[15] Waxes on Lotus leaf reduce the SFE, while micro and nano structures maintain the air pillows resembling Cassie-Baxter model.[16]. The trapped air, between liquid and solid interface, forces the liquid drop to form spherical shape supported by the surface tension of a liquid. The low surface free energy is fully ensured by the organic waxes. This was proved by washing waxes with acetone, which led to considerable reduction of water CA.[14] Other examples of SHP surfaces in nature include wings of some butterfly species, cicada wings, shark skin, which also have microstructures on their surfaces ensuring self-cleaning, anti-bactericidal SHP effects.[4]

1.4. Artificially made superhydrophobic surfaces

It is not a secret, that artificially SHP surfaces can be made by increasing surface roughness and (or) reducing surface free energy of untreated surface. Usually for low SFE surface, the right choice of substrate material is essential, however artificially SFE can be reduced by means of chemical coatings. Carbon soot SHP surface is one of the easiest to make due to simple methodology, accessible materials, yet water drops remove the soot layer leading to its degradation.[17] Another method to increase surface roughness uses photolithography to transfer a pattern of microstructures on a substrate by irradiating a photoresist by light. It was demonstrated that additional coating of such microstructures on silicon by Lotus waxes produces CA of about 173°.[18] Metals are also used as a substrate material for creation of artificial SHP surfaces. They can be easily textured by laser and this processing delivers CA of 158° on steel surface.[19] Chemically, SHP surface can be made by dipping a substrate in the solution, which can be made by sol-gel process and one of such surfaces on glass exhibit CA of 158° with transparency, that would be suitable for niche applications.[20]

1.5. PTFE polymer

Polymers are intrinsically hydrophobic materials due to nonpolar bonds and a structure containing long chains of molecules. This feature makes them very suitable materials for water repellent surfaces. The etalon of hydrophobic polymer is polytetrafluoroethylene (PTFE) due to low surface free energy. Self-explanatory PTFE is nonpolar fluoropolymer (Fig. 4), having fluorine atoms strongly bonded with carbon in cyclic chains. Sheets of material are white; less than 1 mm thickness films are partially transparent. Light scattering, and diffusively reflecting properties are used in optics. C–F bonding is strong due to high fluorine electronegativity ensuring low chemical activity, mechanical rigidity, and good thermal properties of PTFE.[21] Sometimes PTFE is referred to Teflon™ as commercially distinguishable denotation. Main applications in industry include low adhesive frying pan layers, cable coatings for electrical isolation, bioimplants and other fields in mechanical engineering.[21] Its spread in domestic applications is attributed to high electrical resistance and low friction coefficient.

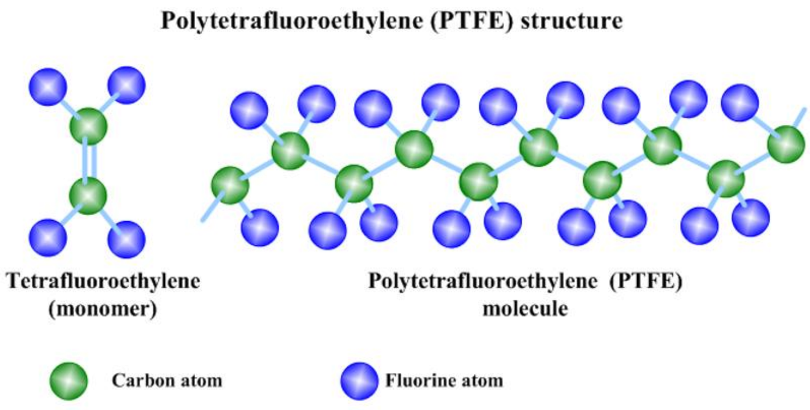

Figure 4. PTFE chemical structure. [22]

Special attention is paid for hydrophobic property of PTFE surfaces caused by low surface energy. Water contact angle on mechanically untreated PTFE surface lies in a range between 110° and 120° depending on measurement accuracy and material surface condition.[23] Additional surface treatment with femtosecond laser induce SHP surfaces having CA of about 166° and sliding angle as low as 2° for water on PTFE.[24] In another study contact angle as high as 170° have been achieved using Ti:sapphire laser at 800 nm wavelength and biaxial scanning approach. The second rescan was done using lower average laser power.[25] Authors also noticed that uniaxial scanning approach creates unidirectional hydrophobicity with lower CA compared to biaxial ones. Surfaces also demonstrated anti-icing behaviour.

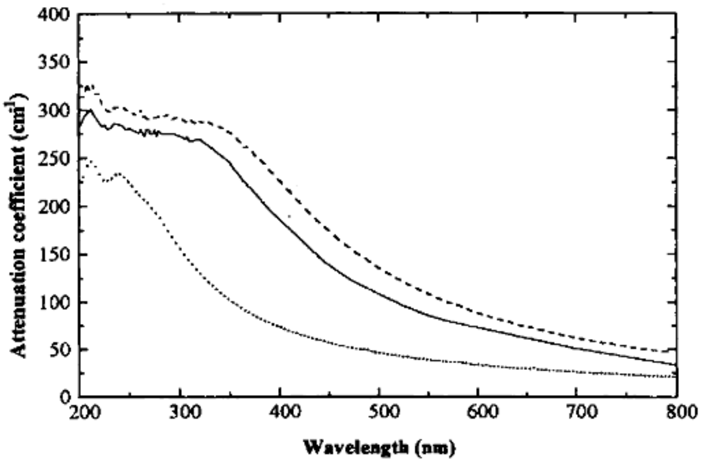

Figure 5. Attenuation coefficient spectrum of three PTFE samples with slightly different chemical morphologies. [26]

PTFE absorption spectra can be seen in Figure 5, where attenuation coefficient is inversely proportional to the wavelength. However, PTFE is transparent in visible spectrum since it does not have any chromophores absorbing specific wavelengths of light and the maximum wavelength of direct electronic transitions is 140 nm.[26] Ferry *et al.* suggests that higher absorption values than expected in UV region can be explained by crystallite scattering phenomena.[26] At UV spectral range picosecond laser micromachining on PTFE surfaces can deliver water CA of about 168° with higher ablation efficiencies compared to fs laser texturing.[27]

1.6. Laser micromachining

Laser micromachining in broad sense can be understood as changing material’s chemical and physical structure by means of laser radiation in the scale of micrometres. Usually, laser is an essential part of machining setup, yet other elements, for instance, beam expander or focusing optics are important as well to achieve high energy densities to make desired impact on material. In laser material processing some parameters are important to take into account regardless type of processing: additive or subtractive fabrication. Single pulse energy can be calculated by dividing the average laser power by pulse repetition rate. Knowing single pulse energy, dose of sum energy incident on material can be further calculated. The total energy incident on material, when laser beam moves along the sample surface, can be calculated knowing the total laser beam distance travelled along the sample:

$$E_{total} = P\,\frac{S_{total}}{v}\,, \tag{4}$$

Here P – laser power, v – laser scanning velocity, S_{total} – total laser beam distance travelled on sample surface. In order to determine how individual pulses arrange in space on sample (Fig. 6a), the overlap definition is used. The overlap between two separate pulses is calculated from an overlap ratio of next pulse edge on previous diameter. Distance of ω_0 between adjacent pulses refers to -50 % overlap (Fig. 6b), while 0 % overlap indicates pulses being contiguous to each other (Fig. 6c).

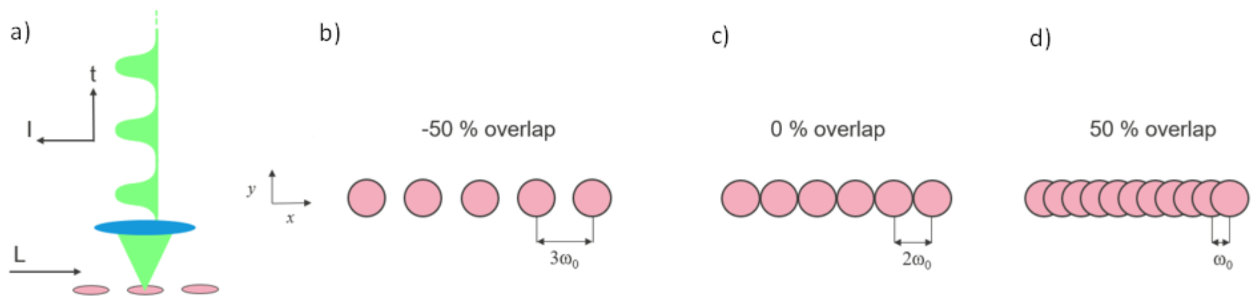

Figure 6. Definition of laser pulses: a) layout in space and time b) overlap parameter of -50 % c) overlap parameter of 0 % d) overlap parameter of 50 %.

Another important parameter in laser micromachining is fluence or energy density, which is single pulse energy incident on effective focal spot area. It is calculated using the following formula:

$$\Phi = \frac{2E_P}{\pi\omega_0^2}, \quad (5)$$

here ω_0 – spot size radius, E_P – energy of a single pulse. This quantity is usually expressed in J/cm^2. The smaller spot size results in larger fluences and higher intensities for the same radiant optical energy. By varying spot size or pulse energy, material can be either damaged or not. Another important parameter is ablation threshold, which is unique for every material and expressed as energy density. In general, it is the minimum energy density required to induce material removal.[25] For PTFE ablation threshold fluence is around 0.3 J/cm^2 for UV fs laser pulses.[28] The ablation threshold fluence and beam waist diameter can be found using Liu's method: the square of laser ablated crater diameter is plotted against logarithmic laser pulse energy.[29] Using linear function fit, laser beam waist diameter can be found from line slope $a = 2\omega_0^2$ of dependence in formula (6) and material ablation threshold represents function intersection with abscissa.

$$D^2 = 2\omega_0^2 \ln\frac{E}{E_{th}}, \quad (6)$$

1.7. Femtosecond laser pulses interaction with matter

When light penetrates the surface of the matter, electrons are the first to absorb the energy of incoming photons. This process is sometimes called inverse *bremsstrahlung* effect**.** Before the optical energy reaches the lattice or specifically atoms nuclei, there exists two temperatures in material not at equilibrium: lattice and fast electrons. The time when energy is transferred from excited electrons to the lattice is called thermalization duration (τ).[30] After this period equilibrium between lattice and electrons starts to appear – the optical energy as heat dissipates in the material. Thermalization duration lies in range of picoseconds and is unique for different materials, thus absorption of ultrashort laser pulses (fs - ps) by the electrons ends before possible thermalization events. Material interaction with long pulses (ns - μs) results in thermal side effects: remelted zones, debris, cracks and etc. (Fig. 7a). On contrary, fs laser micromachining has fewer side effects during material removal and allows to perform more precise cuts (Fig. 7b). Moreover, using fs pulses it is possible to avoid plasma formation near the surface of processing zone, this allows to avoid additional absorption effects.[31] 'Cold ablation' is another term used to denote material removal from the surface using fs laser pulses when no thermal effects are involved during the interaction processes.[32] Besides, cold ablation may refer to micromachining using lasers with wavelengths at UV range. These photons usually have more energy than chemical bonding energy and molecules are disrupted by breaking the bonds inside them. Material is ablated or removed from bulk as disrupted material is evaporated from its constituents and no heat dissipation process is involved.

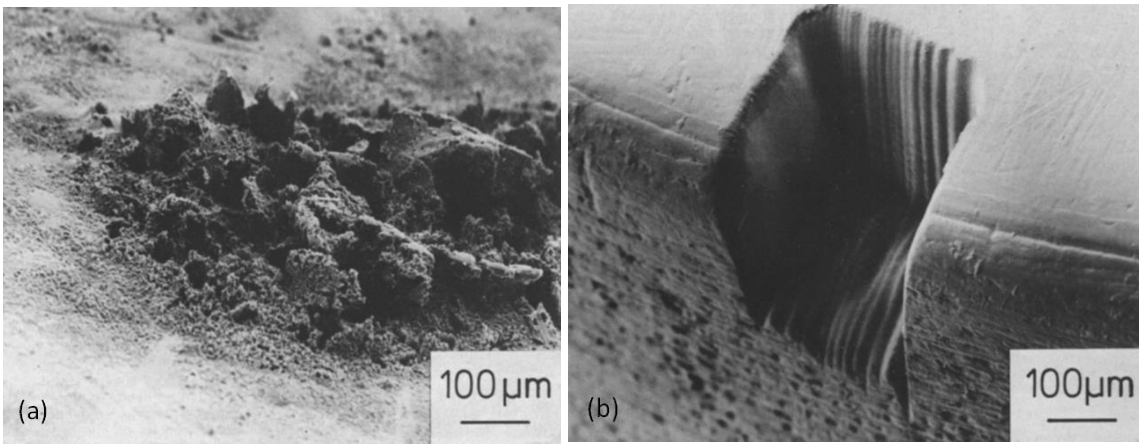

Figure 7. Ablated PTFE surface with 248 nm and laser pulse duration of: (a) 16 ns and (b) 300 fs. [33]

1.8. Multiphoton absorption in laser ablation

There is difference between different light intensities and what it makes to matter during the interaction process. In everyday life light and matter interaction is said to be linear, meaning that material polarisation responds to oscillating electric field strength linearly. The parameter describing material response to light is an average material dipole moment per unit volume. The incoming electromagnetic wave forces electric charges of the dielectric matter to oscillate at the same frequency as the electric field strength of the wave. This refers to material polarization and it obeys linear law with an increment of susceptibility coefficient. When exposed to high intensity laser radiation, material exhibits nonlinear polarization dependence on electric field.[34]

$$P(t) = \epsilon_0\chi^{(1)}E(t) + \epsilon_0\chi^{(2)}E^2(t) + \epsilon_0\chi^{(3)}E^3(t) + \ldots = P_L + P_{NL} \quad , \tag{7}$$

Here $P(t)$ – material polarisation, ϵ_0 – absolute dielectric permittivity, $\chi^{(n)}$ – nth order optical susceptibilities, $E(t)$ – electric field strength, P_L – linear polarization, P_{NL} – nonlinear polarization. This is explained by induced higher order susceptibilities, which can be useful for various nonlinear effects: higher harmonic generation, Kerr effect, multiphoton absorption and more. When light electric field is comparable to internal electric field of the molecule and phase matching criterium is fulfilled, the generated material dipoles oscillate coherently and cause nonlinear phenomena to appear.[34] In material processing another nonlinear effect is present when more than one photons are absorbed in material via virtual energy levels. The sum energy is equal or higher than bandgap of semiconductor or dielectric materials (Fig. 8).

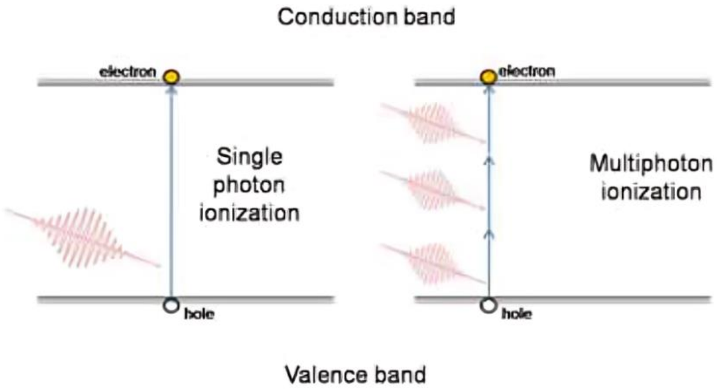

Figure 8. Single photon absorption (left) and multiphoton absorption (right) events via virtual levels leading to ionization of the semiconductor material. [35]

In organic substances, this energy is equal or higher than the energy difference between ground and excited singlet states. Femtosecond laser pulses have high peak powers; thus, utilization of fs micromachining technology enables transparent material ionization with high energy bandgap (> 3 eV) even in visible and NIR wavelengths.[36] Material is said to have nonlinear absorption.

As discussed in 1.5 section, PTFE is transparent fluoropolymer with chromophores of less than 140 nm wavelength. Thus, poor ablation in visible light region is observed using Q-switched laser oscillators. Femtosecond lasers induce multiphoton absorption mechanism on PTFE, which leads to decomposition of long polymer chains to smaller particles, which is hard to achieve with ns lasers. [37]

Knowing the properties of superhydrophobic surfaces and physics beyond them allows to choose material and methods for this work. For successful fabrication of SHP surface low surface free energy polymer is used together with fs laser texturing to increase average surface roughness. The synergy of these two properties might result in contact angles above 150°.

2. Materials and experimental methods

2.1. Samples

Several substrates of polytetrafluoroethylene with thickness of 3 mm were used. The density of PTFE plates is 2.2 g/cm^3, melting temperature ~300°C. Prior the fabrication procedures samples were washed with deionized water and blown with ‘Thorlabs’ air duster for removal of any solid contamination to avoid unnecessary absorption or scattering effects, which could influence the ablation efficiency.

2.2. Laser machining setup

The solid-state air-cooled laser system ‘Carbide’ manufactured by ‘Light Conversion’ Ltd. (Lithuania) was used as 515 nm central wavelength light source during microfabrication procedure. The system delivers 220 fs pulse duration and second harmonic central wavelength of 515 nm at 60 kHz repetition rate. The principle optical scheme is represented in Figure 9a.

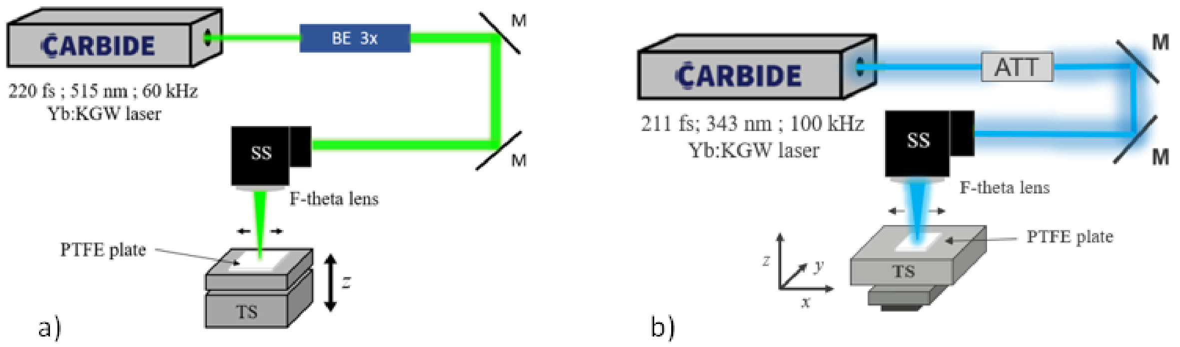

Figure 9. Schematic diagram of PTFE laser micromachining setup using a) 515 nm wavelength b) 343 nm wavelength. Here, BE – beam expander, M – mirrors, SS – galvanometric scanner system, TS – translational stage, ATT – power control unit.

The laser beam exiting the laser unit emanates through the beam expander with magnification of 3 times. Afocal system consists of two lenses forming Galilean design: concave (f = -50 mm) and convex (f = 150 mm). Then, beam is directed to the scanner system (Scanlab ‘intelliSCAN 14’) by mirrors. Scanner system consists of two galvanometric mirrors capable of moving the laser beam on the translational stage in x and y directions. The beam is focused on the sample using ‘Linos’ f- theta lens having focal length of 100 mm for 515 nm wavelength. The sample is placed on the single axis translational stage (Thorlabs ‘MLJ150/M’). The height of stage in z axis and thus the focal position of the beam on the sample was adjusted using the ‘Kinesis’ software by ‘Thorlabs’ via PC. The algorithms of the laser beam motions with this laser system were written with ‘SCA’ system control software and controlled by PC.

As UV light source, laser system ‘Carbide’ by ‘Light Conversion’ Ltd. was used having 343 nm central wavelength and 100 kHz pulse repetition rate with pulse duration of 211 fs. The principle optical system with 343 nm light source can be seen in Figure 9b. Laser beam power is controlled with polarization adjust unit. Then, laser beam is directed to the scanner system ‘Scanlab intelliSCAN 14’ using mirrors and focused using ‘Linos’ *f*-theta lens (f = 100 mm) for 343 nm wavelength. Sample is moved in *xyz* directions using automated ‘Aerotech’ stages. Laser scanning algorithm was written, and laser setup was controlled by ‘DMC’ software with PC.

2.3. Scanning techniques

The laser scanning techniques should deliver micro-scale surface irregularities to induce air gap between water drop and bulk material to trigger SHP water CA regime. Moreover, hydrophobic properties should be directionally independent on the surface, thus orthogonal algorithms are needed. The laser scanning algorithm for constant depth areas was written to process square shape sectors with constant parameters: laser scanning velocity (v) or beam overlap, distance between adjacent scanning lines (d_{period}) and number of biaxial rescans (s). One biaxial scan consists of two uniaxial scans each having multiple parallel grooves with equal distance between adjacent ones as seen in Figure 10. Both uniaxial scans are aligned in such manner that orthogonality between grooves of first and second scan is ensured.

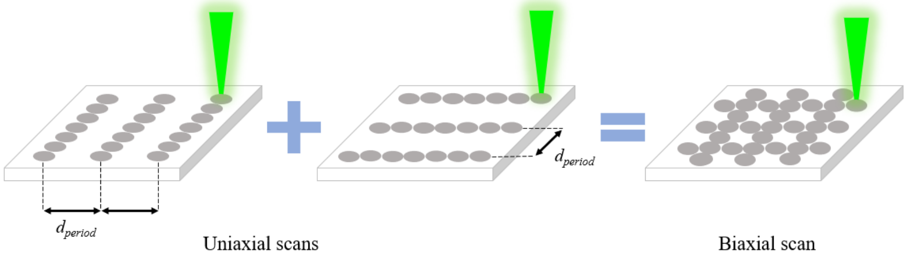

Figure 10. Biaxial scanning technique with multiple parallel grooves in perpendicular directions. Arrangement of pulses resembles 0 % overlap in scanning direction.

To increase the depth of the whole area under micromachining, either the number of (biaxial) scans is increased (Fig. 11) or d_{period} and v are reduced. To avoid (de)acceleration of laser beam at the boundaries of the straight trajectory, function ‘skywriting’ in SCA program is used to avoid energy accumulation areas leading to deeper hollows.

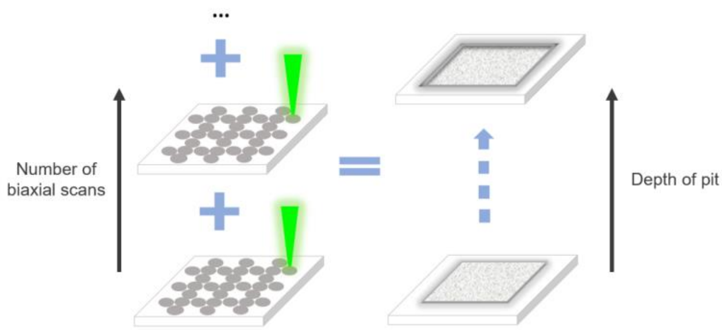

Figure 11. Effect of increasing number of biaxial scans to the increasing depth of the laser micromachined area.

2.4. Measurements

The surface morphology was inspected using optical surface profiler (‘PLu 2300’) by ‘Sensofar’. The 3D surface data were analyzed with ‘Gwyddion’ program. The parameter under investigation of detailed ablated surface area was average surface roughness (R_a). Reflectivity of PTFE in visible spectrum range is low compared to metals, thus optical measurements may be measured inaccurately due to lack of data points or induced artifacts. To avoid this during the surface imaging, after the microfabrication samples were coated tens of nanometers either silver or gold layer via sputtering device in inert environment (‘Quorum Q150’).

The images of detailed surface structures were taken using tabletop Scanning Electron Microscope (SEM) ‘Hitachi TM-1000’. All the observed samples were also coated with a few tens of nanometers of silver or gold layer to reduce charge accumulation for better imaging.

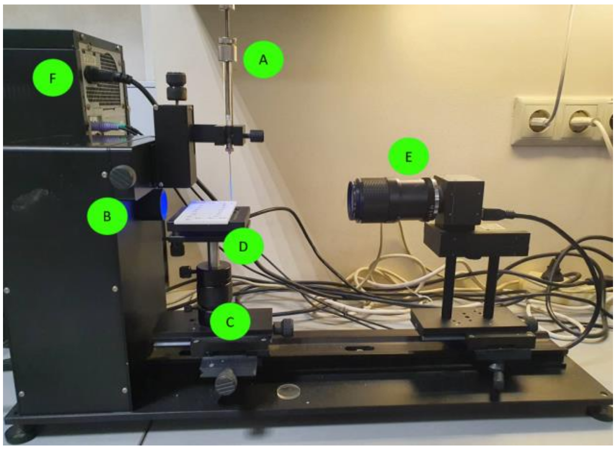

Figure 12. KSV CAM 200 contact angle measurement setup scheme. A – precise syringe for water drop formation, B – light source, C – sample positioning and alignment stage, D – PTFE sample under measurement, E – objective and camera sensor, F – PC for data processing.

For precise water contact angle measurements 'KSV CAM 200' setup located at Vilnius University Institute of Chemistry was used (Fig. 12). This setup enables to measure exact volume of liquid with excellent lighting conditions for accurate measurements. Precise leveling of the sample was necessary to avoid droplet rolling off the surface for stable imaging. The image of water drops on PTFE samples have been processed by 'Attension theta' program.

To determine the same laser pulses overlap parameter for two different laser wavelengths, the laser beam waist radii are calculated using Liu's method performed on metal surface by plotting square of measured crater diameter (*D*) dependence on laser pulse energy (*E*) at logarithmic scale as written in section 1.6. The linear fit of data sets gives out a slope coefficient equal to the double square of laser beam waist radius as seen in Figure 13. The laser beam waist for 515 nm wavelength was 21.8 μm, for third harmonic generation (343 nm) it was equal to 10.5 μm.

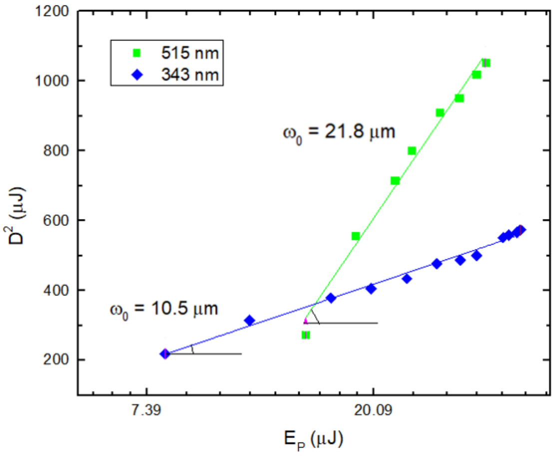

Figure 13. Graph of square of ablated diameter versus laser pulse energy for laser beam waist radius determination using Liu's method.

3. Results and discussion

Firstly, to determine ablation efficiency three sets of samples with different scanning velocities of v_1 = 550 mm/s (80 % overlap); v_2 = 900 mm/s (65 % overlap); v_3 = 1350 mm/s (50 % overlap) were fabricated by varying number of biaxial scans (s) and period (d_{period}) using 515 nm wavelength (Fig. 14). As expected, the measured maximum depth of ablated squares increases along with number of scans and decreases with period.

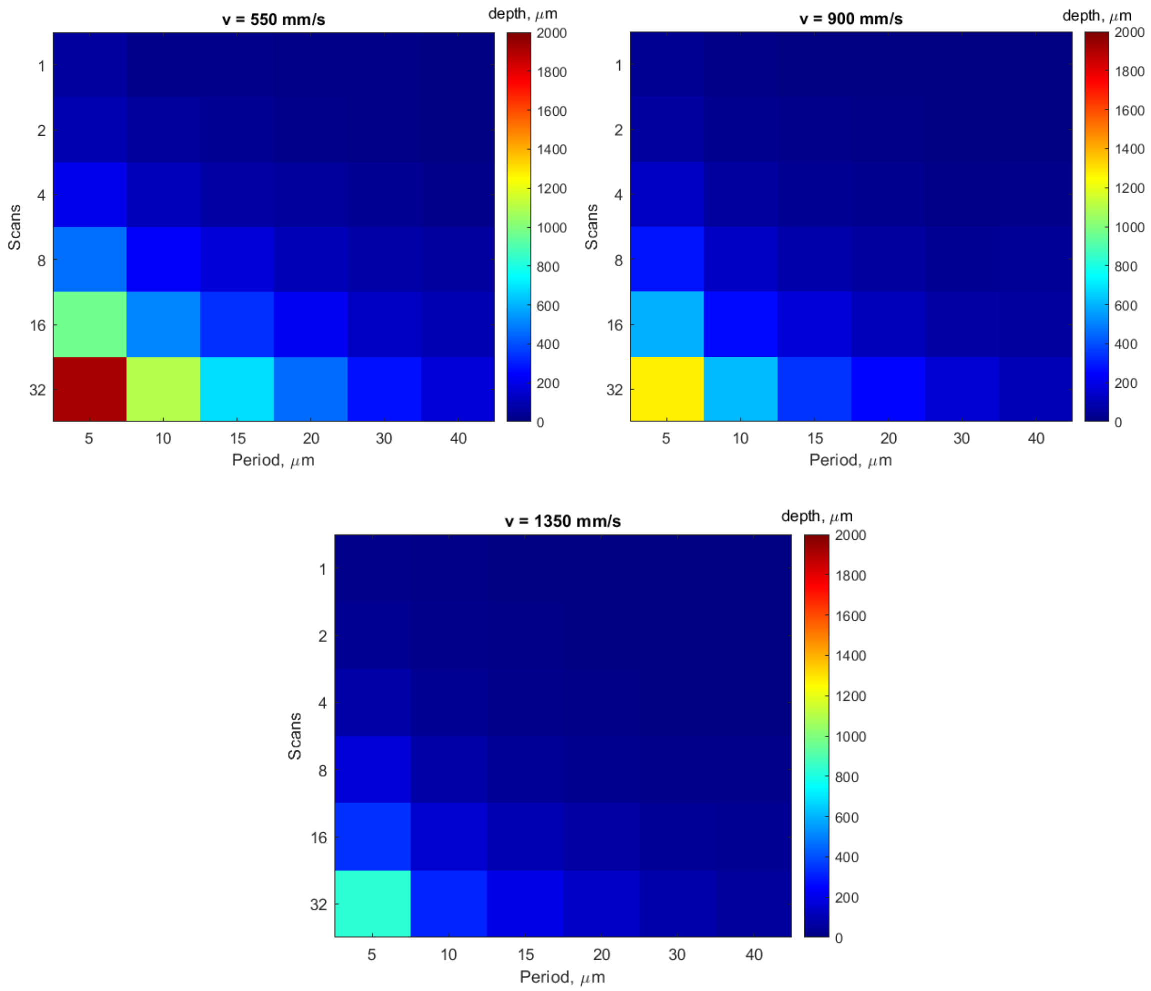

Figure 14. Maximum depth of ablated pits dependence on number of scans and scanning period for three velocities using 515 nm wavelength.

The tendency of depth increase was similar for all three scanning velocities, but the absolute values of depths were the highest for v_1 = 550 mm/s and lowest for v_3 = 1350 mm/s. This is obvious from the point of view, that lower velocity leads to higher density of laser pulses and consequently overlap along the scanning trajectory. The deepest pit depth was measured to be approximately 1915 µm with scanning parameters: v = 550 mm/s; s = 32 and d_{period} = 5 µm. The pit of square shape has deepening slope from the edges towards the center with lower ablation rate at boundaries on the square perimeter (Fig. 15).

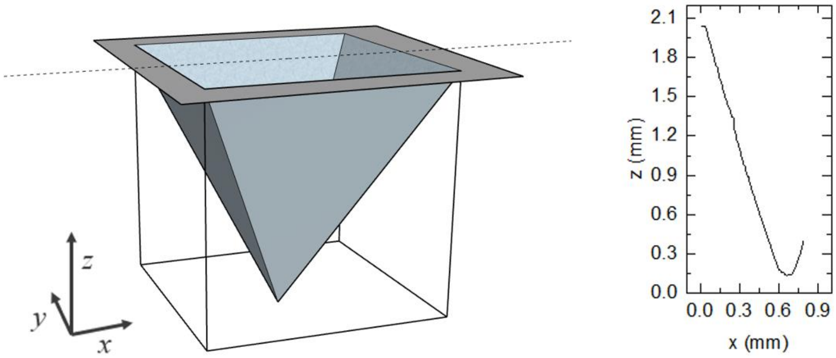

Figure 15. 3D model of the deepest cavity resembling inverse pyramid shape pit. Dotted line indicates cross-section of the profile depicted on the right. Axes scales are equal. (v = 550 mm/s, 80 % overlap, d_{period} = 5 µm, s = 32, λ = 515 nm)

Hence, the shape of removed material volume in Figure 15 resembles square pyramid figure. The lower ablation efficiency at the periphery of a square can be explained by increased projected area of a laser beam on the sample when beam is incident at nonzero angle to the surface, which leads to lower energy density. Thus, only the centre part of the square maintains higher ablation rate compared to the surroundings. Significant pattern of ordered protrusions for higher scanning periods were seen as a result of laser scanning trajectories (Fig. 16). The surface roughness of micro-scale surface protrusions was R_a = 4.5 µm. The step at the edges may be due to misalignment of perpendicular x and y directions uniaxial scans caused by laser scanning software or scanner system hardware peculiarities. This indicates that scanning algorithm function 'skywriting' did not work completely.

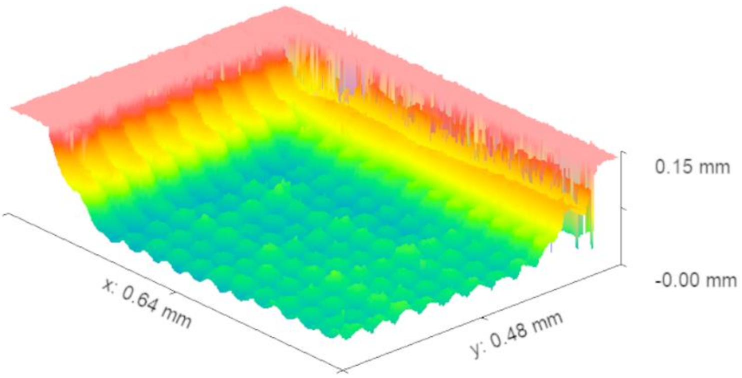

Figure 16. Surface profile of pit with observable laser beam scanning trajectory. (v = 550 mm/s, 80 % overlap, d_{period} = 40 µm, s = 32, λ = 515 nm)

Removed material volume divided by total laser energy incident on area under ablation (ablation efficiency) dependence on scanning period and number of scans is plotted for all three scanning velocities using second harmonic generation (Fig. 17). The sample areas under ablation are squares of 1 mm for each side. The highest amount of ablated material volume was achieved with v = 550 mm/s, s = 32 and d_{period} = 5 µm having ablation efficiency of about 0.015 mm^3/J.

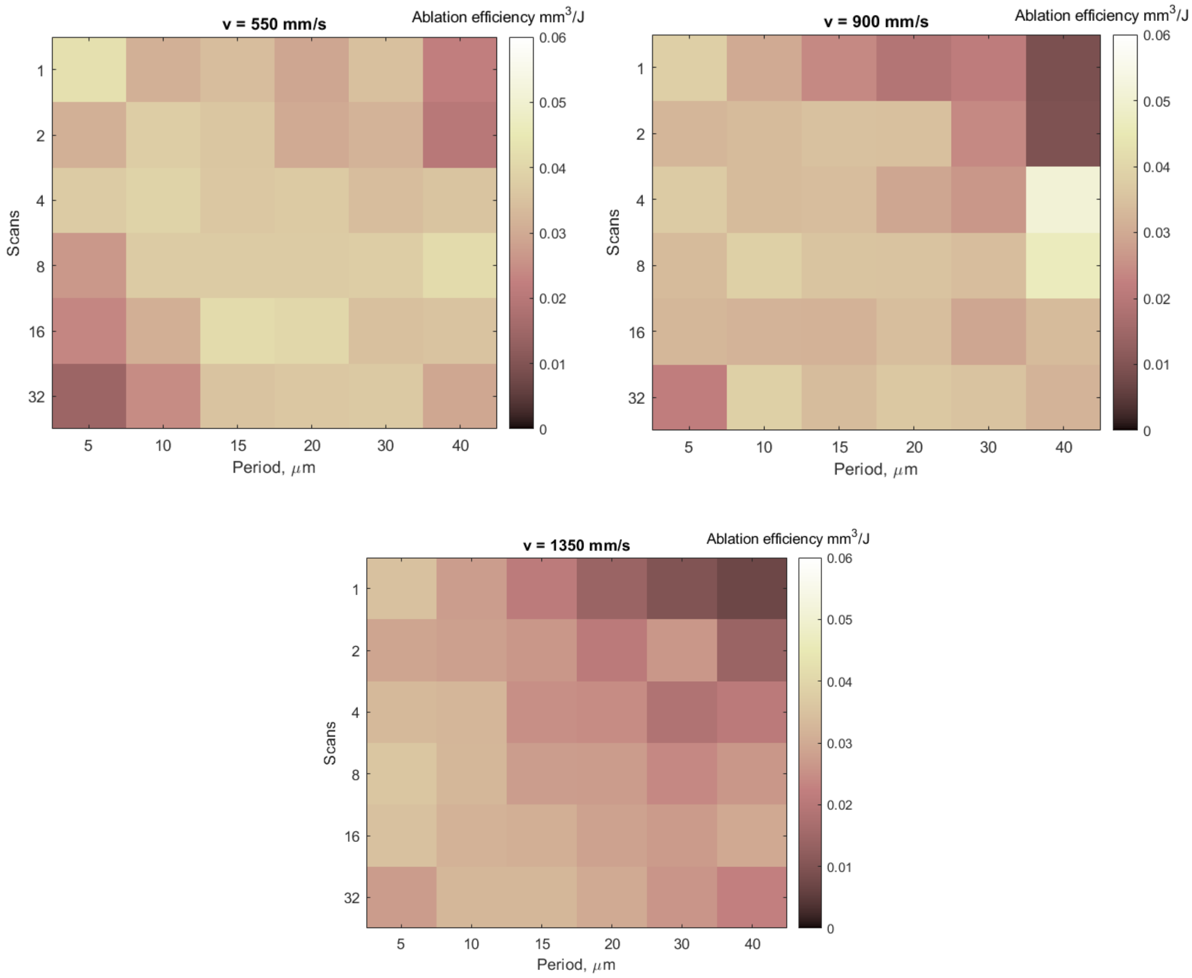

Figure 17. Ablation efficiency dependence on period and scans for three laser beam scanning velocities using 515 nm wavelength.

Since at lower ablated depths beam projected area has low deviations from smallest beam spot size on flat surface, the slopes at the edges of the pits are negligible. However, for total energies absorbed by material above 12 J, the ablated volume of pits starts to saturate, and pits has ablated volume shape of truncated pyramid. The volume of ablated material for truncated pyramid shape hollow was calculated by formula:

$$V = \frac{H(a^2 \cdot b^2 + ab)}{3}, \quad (8)$$

Where a – side of larger baser of pyramid (in this case 1 mm); H – truncated pyramid height (depth of pits with slopes); b – side line of smaller base of pyramid (side of smaller base square in the bottom of ablated area). For the deepest hollow with square pyramid-shaped surface profile (Fig. 15), the ablated volume was calculated with the following formula:

$$V = \frac{a^2 \cdot H}{3}, \tag{9}$$

Where a – pyramid base length (1 mm); H – pyramid height (the deepest place of pit, which equals to 1915 μm). There is no significant dependence pattern of ablation efficiency. However, lower efficiencies are found at high number of scans and low periods due to pyramid-shape ablated volume, and for low number of scans and high periods since larger period leaves unaffected material between adjacent scans similar as in Figure 16. Moreover, ablated volume determination for depths lower than 5 μm are inaccurate due to low height differences between untreated surrounding surface and the pit. The higher absolute efficiency is achieved using highest scanning velocity of v = 550 mm/s (80 % overlap), because it delivers more energy on the material. The lowest absolute ablation efficiency values are achieved using v = 1350 mm/s.

Extensive research on CA dependence on laser fabrication parameters have been conducted using flat textured surfaces. Laser micromachining parameters for two laser wavelengths at flat surface texturing are shown in Table 1:

Table 1. Laser micromachining parameters for flat PTFE superhydrophobic surfaces.

λ	**Pulse duration (fs)**	**Pulse repetition rate (kHz)**	**Spot size radius (μm)**	**Average power (W)**	**Fluence (J/cm^2)**	**80 % overlap scanning velocity (mm/s)**	**65 % overlap scanning velocity (mm/s)**	**50 % overlap scanning velocity (mm/s)**
343 nm	211	100	10.5	0.76	4.4	416	728	1040
515 nm	220	60	21.8	1.97		550	900	1350

Although both lasers, and consequently wavelengths, have different parameters and focusing conditions, the fluence and overlap of pulses are set to be equal by other parameters for both laser systems. In Figure 18 CA dependence on period is plotted for 343 nm and 515 nm wavelengths using three numbers of biaxial scan algorithms for three pulses overlap values. Talking about 1 rescan graphs, for UV radiation CAs for all overlaps are higher for 30 μm and 50 μm periods compared to 10 μm and 70 μm periods except one artifact at 65 % overlap. For 515 nm wavelength remarkable dependence is not observed for 65 % and 50 % overlaps, whereas for 80 % overlap CA increase with period. The highest CAs are reached using 50 % overlap for both wavelengths. For 343 nm all periods demonstrate CA above 166° with the highest value of 171° (d_{period} = 50 μm). Only two CA for UV radiation are not considered as SHP (CA < 150°) having 80 % overlap for (d_{period} = 10 μm and d_{period} = 70 μm).

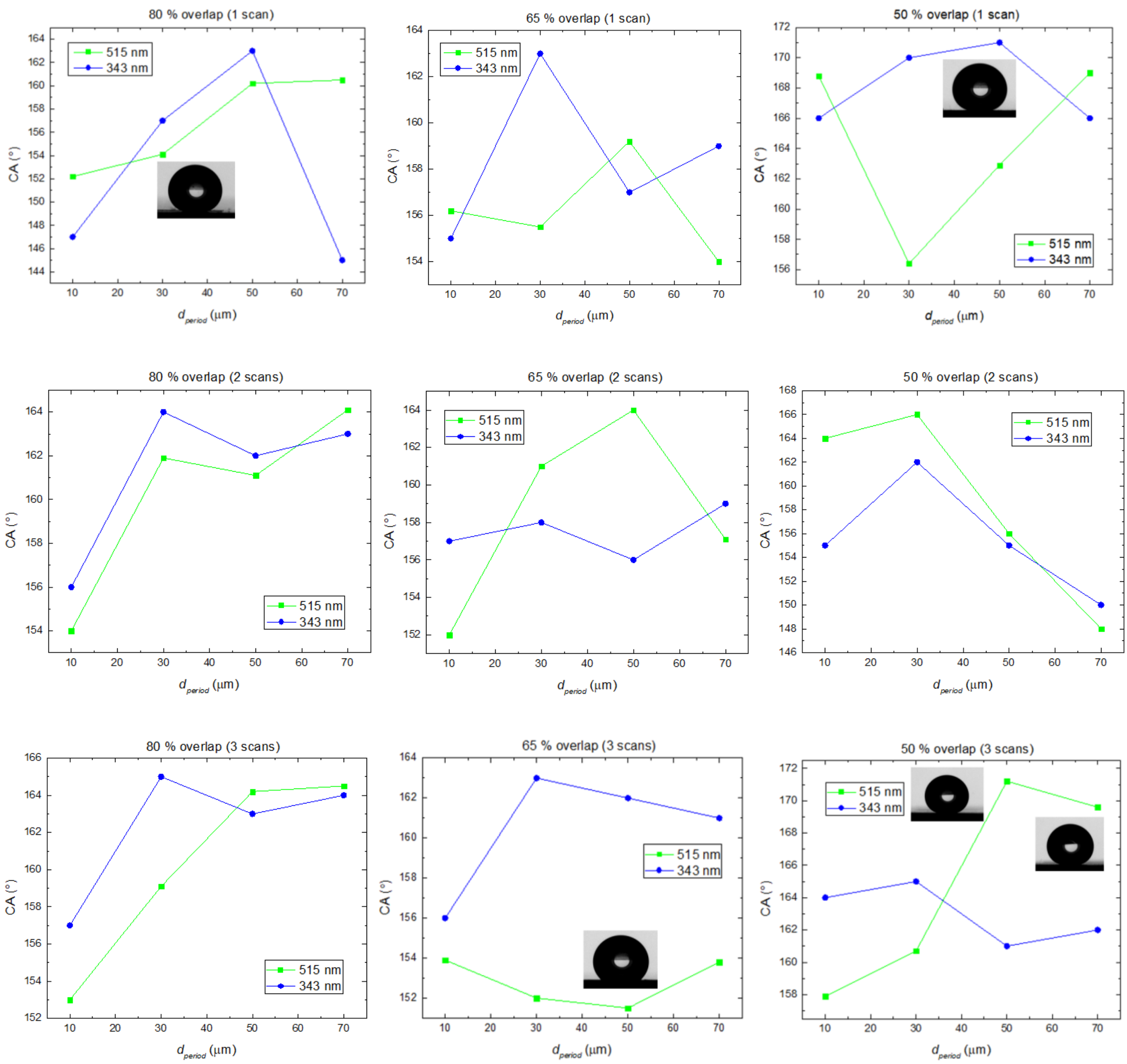

Figure 18. Water CA dependence on scanning period for flat surfaces using two laser wavelengths for 80 %, 65 % and 50 % overlap of pulses and for 1; 2 and 3 biaxial scans.

Talking about plots having 2 rescan parameters (Fig. 18), dynamics of 343 nm and 515 nm is much more similar for 80 % and 50 % overlap, especially for 80 % overlap the absolute CA values differs only a few degrees. The only CA value below 150° line belongs to 515 nm (50 % overlap) contrary to 1 biaxial scan indicating that 2 biaxial scans have higher probability to deliver superhydrophobic surface. For 2 biaxial scans for each overlap value the highest contact angles were measured for second harmonic generation laser texturing. The highest contact angle using 2 biaxial scans is 166° (50 % overlap; d_{period} = 30 μm; λ = 515 nm).

3 biaxial scans have been implemented using a set of overlap values (Fig. 18). For 80 % overlap the tendency is similar to 2 number of scans for the same overlap. For 515 nm wavelengths (80 %

overlap) the CA increases as period increases for 1 and 3 numbers for rescans. The significant difference of results between laser harmonics for all fabrication parameters can be seen at 65 % overlap and 3 scans, where 343 nm wavelength possess more than two degrees higher CA values for a range of scanning periods. The highest contact angle using 3 biaxial scans is captured to be 171° (50 % overlap; d_{period} = 50 µm; λ = 515 nm).

To sum up, the majority of measured CA values are SHP and there is only one set of CA against period values (65 % overlap and 3 scans), where there is significant difference between laser harmonics at all periods. Remaining sets of parameters show alternating higher CA domination of both laser harmonics. The overall highest value (CA_{max} = 171°) was achieved using both 343 nm and 515 nm laser wavelengths with fabrication parameters (50 % overlap; d_{period} = 50 µm; 1 biaxial scan) and (50 % overlap; d_{period} = 50 µm; 3 biaxial scans) respectively. For final evaluation, laser scanning time should be also taken into account. The time to texture PTFE surface with 515 nm wavelength takes 3 times more time compared to 343 nm for the same result of CA_{max} = 171° as 1 biaxial scan is more time-effective than 3 biaxial scans. Thus, the optimal fabrication parameters for texturing PTFE surface to achieve the best superhydrophobicity are 343 nm laser wavelength, d_{period} = 50, 1 biaxial scan and 50 % overlap corresponding to v = 1040 mm/s. These parameters are compatible with laser spot size of ω_0 = 10.5 µm. Achieved maximum contact angle is one of the highest to this date using fs laser texturing on PTFE material with second and third harmonic wavelengths.

In order to understand surface morphology impact on its wettability, CA against surface roughness parameter is plotted in Figure 19 for two laser wavelengths. Areas were chosen with different scanning periods and number of rescans to obtain different possible roughness values. Average surface roughness parameter was measured for equal 150 mm x 150 mm areas.

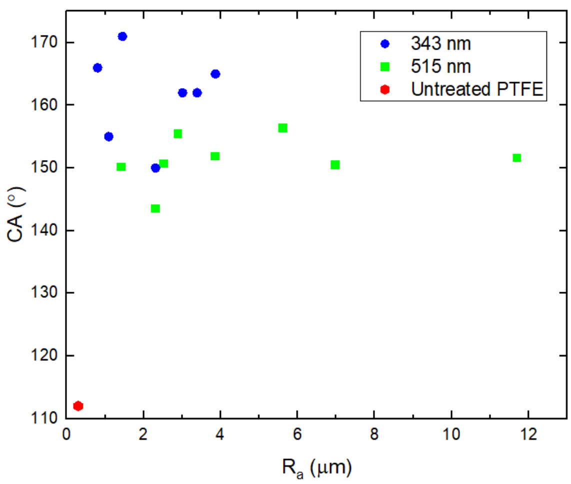

Figure 19. Water CA dependence on average surface roughness for both harmonics. Untreated PTFE surface CA is shown for reference.

From Figure 19 it was noticed that second harmonic generation is capable of producing wider range of surface roughness values compared to the third harmonic. This can be explained by approximately two times wider spot size radius producing larger scale waviness for the same periods. Even larger period of d_{period} = 70 μm and s = 3 for 343 nm wavelength textured area, which is expected to produce high surface roughness, have R_a = 3.4 μm. Since third harmonic generation produce on average smaller surface roughness, it delivers higher water contact angles for similar R_a compared to second harmonic. It may be caused by specific material structure modification after interaction with 343 nm wavelength. Nevertheless, all laser textured surfaces have over 30° higher CAs compared to bare PTFE surface CA of 112° (Fig. 20). This implies that surface roughness has significant impact to superhydrophobic surface formation.

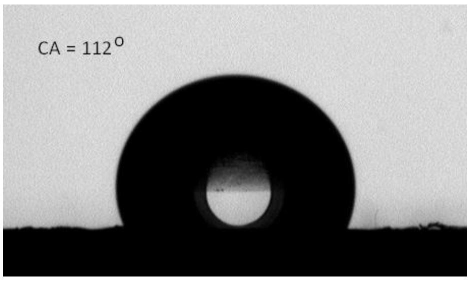

Figure 20. Water drop image on bare PTFE surface for CA determination.

SEM images were taken to qualitatively inspect textured PTFE surface changes and compare between different laser harmonics. In Figure 21 two surface profiles (left λ = 343 nm, right λ = 515 nm) sharing the same CA of 171° are seen. In all images sponge-like fiber structures are visible in the areas under laser impact. These may form nanoscale surface roughness similar to those of Lotus leaves wax clusters (hundreds of nm), which are important to hydrophobic properties. These structures of nanofibers differ between harmonics impact as for 343 nm nanofeatures seem to be sparse and vacant compared to 515 nm laser induced nanofeatures, which look more densely packed (Fig. 21). However, these small surface features were not visible in surface profiler images and consequently measured R_a parameter does not include them. There can be seen bumps of untextured material covered with debris. Trenches of laser impact starts to appear with two and higher number of rescans. The surface made with third harmonic in Figure 21 has height difference between flat top and bottom of pit of ΔZ_{AB} = 1.5 μm and R_a = 1.36 μm, while the surface made with second harmonic of ΔZ_{CD} = 20 μm and R_a = 5.4 μm. This indicates that second harmonic SHP properties are achieved via high surface roughness, whereas third harmonic creates low R_a, but induces unique nanoscale surface texture, which may highly contribute to SHP properties comparable to second harmonic impact.

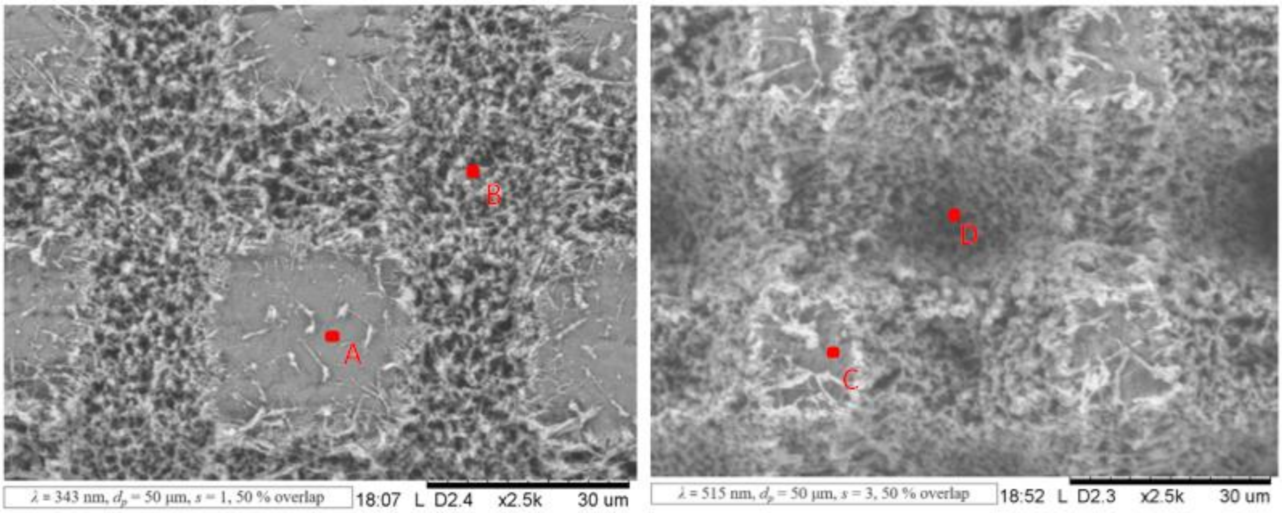

Figure 21. SEM images of textured PTFE surfaces with common CA = 171°. Height differences between points AB and CD are 1.5 μm and 20 μm respectively.

In Figure 22 both surfaces lack untextured zones since period is smaller than in Figure 21. These areas have similar R_a of about 3 μm and common CA of 162°. The microscale surface roughness is formed by repetitive laser scanning grooves together with nanoscale roughness induced by laser radiation impact and surfaces lack untextured zones. Nanoscale fiber structures are similar to those in Figure 21 for the same laser wavelengths.

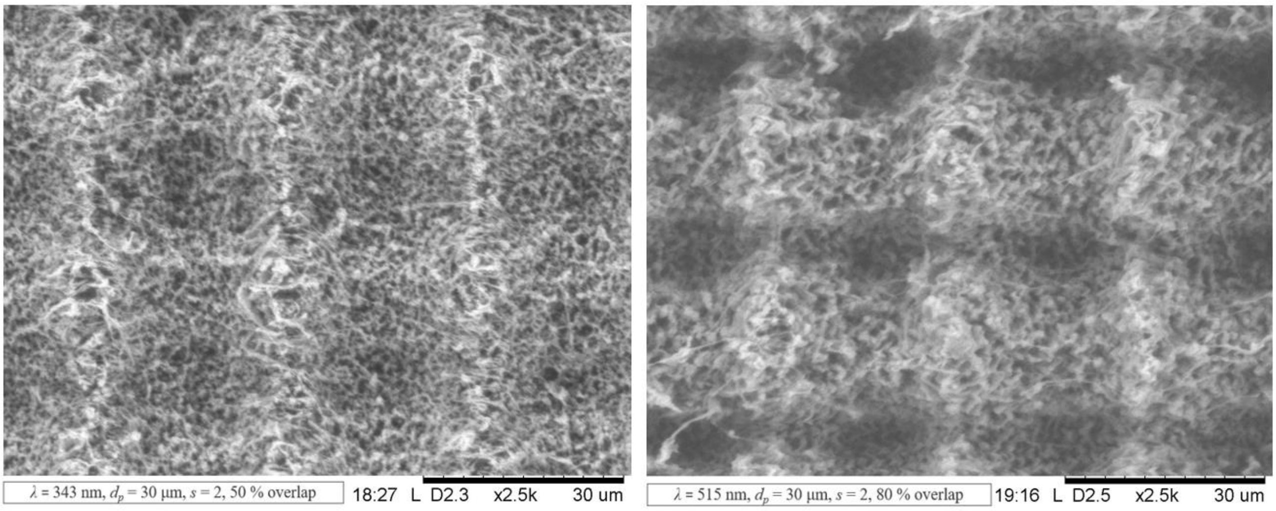

Figure 22. SEM images of textured PTFE surfaces with common CA = 162°.

For an additional task, triangular profile pits were designed to confine water along single direction. To create triangle depth profile samples, the width of the ascending biaxial scans is supposed to be reduced gradually along one axis to deepen the pit respectively (Fig. 23). Increasing the number of scans, the depth of the trench increases accordingly along with the slope of the depth creating step-like profile. This trench enables to confine a drop of water in one direction movement only.

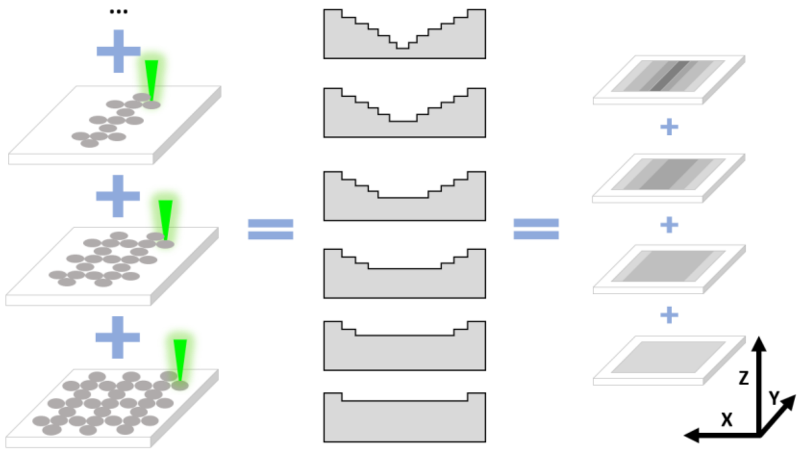

Figure 23. Triangle depth profile laser microfabrication technique.

Triangular profile square-shaped areas confining the water along one direction have been fabricated. The side length of single area is 10 mm. The profile cross-section can be seen in Figure 24:

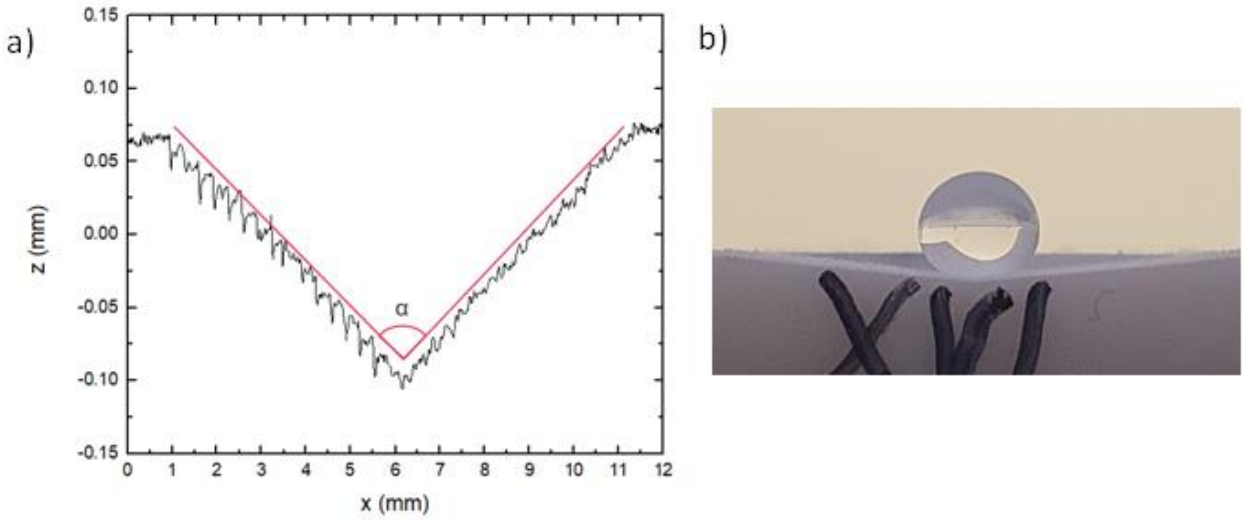

Figure 24. Ablated triangular profile trench a) cross-section with α = 176° and different axes scale (v = 550 mm/s, 80 % overlap, s = 16, d_{period} = 20 μm, λ = 515 nm) b) image of pit with standing water drop.

The slope at left side has repetitive recesses due to laser beam acceleration, whereas at the right the step-like increments are absent (Fig. 24a). These cavities arise due to higher delivered energy density, when the laser beam accelerates during single uniaxial scan resulting in higher pulse overlap values. The total angle formed by the triangle of two side walls is equal to about α = 176°.

Average surface roughness values were measured at the bottoms for triangular profile pits for two different number of biaxial scans as seen in Figure 25a. Absolute values for s = 32 are a bit higher compared to s = 16.

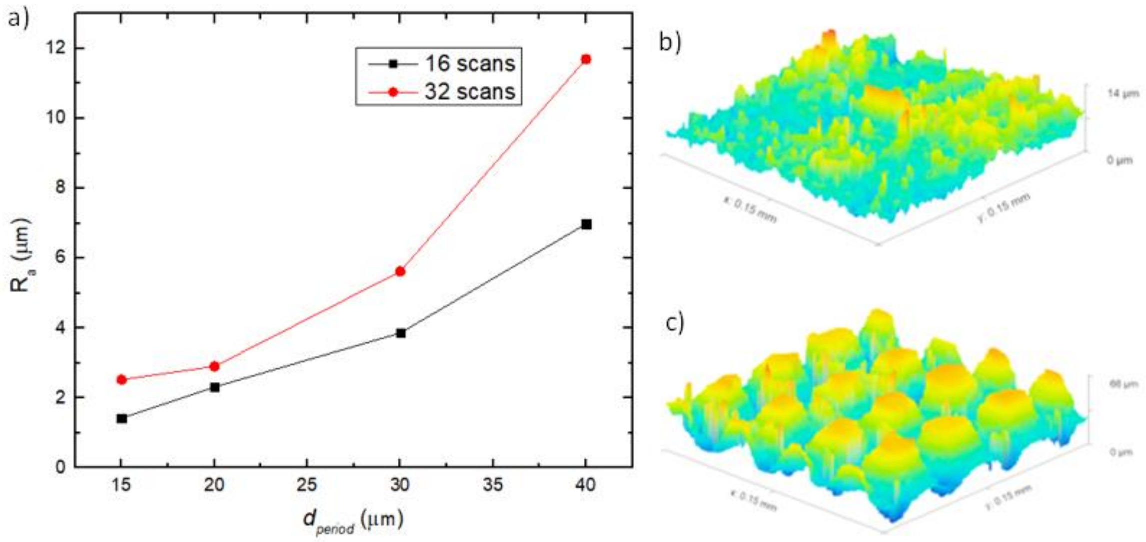

Figure 25. Average surface roughness induced by 515 nm wavelength in triangular profile pits: a) relation on scanning period for 16 and 32 number of scans (v = 550 mm/s) and morphology images with periods b) d_{period} = 15 μm c) b) d_{period} = 40 μm.

There is a tendency of surface roughness increase with scanning period for both number of scans. This can be explained by significant laser beam scanning pattern appearance at higher periods which results in higher surface profile deviations compared to low periods (Fig. 25b and Fig. 25c). However, for s = 32 there are additional surface protrusions arising from triangular depth profile steps creating stair-like height deviations, which increases overall surface roughness similar to Figure 24a. These triangular profiles have superhydrophobic properties as water drops have low sliding angles since drops are hard to be levelled and can roll only in one line. Such triangular profile trenches can be applied to fluid control channels enabling to redirect liquid at predefined direction.

4. Conclusions

1. Laser micromachining using femtosecond laser pulses allows to achieve superhydrophobic surfaces on PTFE polymer by increasing its surface roughness.

2. The highest water contact angles were achieved with both second and third harmonics, reached 171° with optimized processing parameters, which indicates that both harmonics are suitable for superhydrophobicity formation on PTFE surface.

3. However, optimal parameters differ for each laser wavelength: d_{period} = 50 μm; 50 % pulse overlap; s = 3 for 515 nm and d_{period} = 50 μm; 50 % pulse overlap; s = 1 for 343 nm, which implies that third harmonic is more time-effective than second harmonic.

4. The difference in optimal fabrication parameters results in different PTFE surface morphology: using 515 nm laser micromachining superhydrophobicity is created through microscale structures, while UV laser micromachining induces unique nanoscale features.

References

1. U. Hermens, S. V. Kirner, C. Emonts, P. Comanns, E. Skoulas, A. Mimidis, H. Mescheder, K. Winands, J. Krüger, E. Stratakis and J. Bonse, Mimicking lizard-like surface structures upon ultrashort laser pulse irradiation of inorganic materials, Appl. Surf. Sci. **418**, 499–507 (2017).

2. B. Ali, I. V. Litvinyuk and M. Rybachuk, Femtosecond laser micromachining of diamond: Current research status, applications and challenges, Carbon. **179**, 209–226 (2021).

3. L. Jonušauskas, S. Rekštyte, R. Buividas, S. Butkus, R. Gadonas, S. Juodkazis and M. Malinauskas, Hybrid subtractive-additive-welding microfabrication for lab-on-chip applications via single amplified femtosecond laser source, Opt. Eng. **56**(9), 094108 (2017).

4. M. Larrañaga-Altuna, A. Zabala, I. Llavori, O. Pearce, D. T. Nguyen, J. Caro, H. Mescheder, J. L. Endrino, G. Goel, W. N. Ayre, R. K. Seenivasagam, D. K. Tripathy, J. Armstrong and S. Goel, Bactericidal surfaces: An emerging 21st-century ultra-precision manufacturing and materials puzzle, Appl. Phys. Rev. **8**(2), 021303 (2021).

5. N. Nuraje, W. S. Khan, Y. Lei, M. Ceylan and R. Asmatulu, Superhydrophobic electrospun nanofibers, J. Mater. Chem. A **1**(6), 1929–1946 (2013).

6. Y. Y. Yan, N. Gao and W. Barthlott, Mimicking natural superhydrophobic surfaces and grasping the wetting process: A review on recent progress in preparing superhydrophobic surfaces, Adv. Colloid. Interfac. **169**(2), 80–105 (2011).

7. A. M. Kietzig, S. G. Hatzikiriakos and P. Englezos, Patterned superhydrophobic metallic surfaces, Langmuir. **25**(8), 4821–4827 (2009).

8. D. Čereška, A. Žemaitis, G. Kontenis, G. Nemickas and L. Jonušauskas, On-Demand Wettability via Combining fs Laser Surface Structuring and Thermal Post-Treatment, Materials. **15**(6), 2141 (2022).

9. S. Parvate, P. Dixit and S. Chattopadhyay, Superhydrophobic Surfaces: Insights from Theory and Experiment, J. Phys. Chem. B **124**(8), 1323–1360 (2020).

10. Y. Si, C. Yu, Z. Dong and L. Jiang, Wetting and spreading: Fundamental theories to cutting-edge applications, Curr. Opin. Colloid. In. **36**, 10–19 (2018).

11. K. Manoharan and S. Bhattacharya, Superhydrophobic surfaces review: Functional application, fabrication techniques and limitations, J. Manuf. **2**(1), 59–78 (2019).

12. X. Zhang, L. Wang and E. Levänen, Superhydrophobic surfaces for the reduction of bacterial adhesion, RSC. Adv. **3**(30), 12003–12020 (2013).

13. K. Koch, B. Bhushan, Y. C. Jung and W. Barthlott, Fabrication of artificial Lotus leaves and significance of hierarchical structure for superhydrophobicity and low adhesion, Soft. Matter. **5**(7), 1386–1393 (2009).

14. S. Nishimoto and B. Bhushan, Bioinspired self-cleaning surfaces with superhydrophobicity, superoleophobicity, and superhydrophilicity, RSC. Adv. **3**(3), 671–690 (2012).

15. A. Marmur, The lotus effect: Superhydrophobicity and metastability, Langmuir. **20**(9), 3517–3519 (2004).

16. T. Sun, L. Feng, X. Gao and L. Jiang, Bioinspired surfaces with special wettability, Acc. Chem. Res. **38**(8), 644–652 (2005).

17. X. Deng, L. Mammen, H. J. Butt and D. Vollmer, Candle soot as a template for a transparent robust superamphiphobic coating, Science. (1979) **335**(6064), 67–70 (2012).

18. B. Bhushan, Y. C. Jung and K. Koch, Self-cleaning efficiency of artificial superhydrophobic surfaces, Langmuir. **25**(5), 3240–3248 (2009).

19. A. Y. Vorobyev and C. Guo, Multifunctional surfaces produced by femtosecond laser pulses, J. Appl. Phys. **117**(3), 033103 (2015).

20. N. Pratiwi, Zulhadjri, S. Arief, Admi and D. V. Wellia, Self-cleaning material based on superhydrophobic coatings through an environmentally friendly sol–gel method, J. Solgel. Sci. Technol. **96**(3), 669–678 (2020).

21. E. Dhanumalayan and G. M. Joshi, Performance properties and applications of polytetrafluoroethylene (PTFE)—a review, Adv. Compos. Hybr. Mater. **1**(2), 247–268 (2018).

22. 'Polytetrafluoroethylene (PTFE) as solid lubricant [SubsTech]' webpage https://www.substech.com/dokuwiki/doku.php?id=polytetrafluoroethylene_ptfe_as_solid_%20lubricant&s=ptfe%20structure. Accessed 2023 – 01 – 07.

23. S. W. Fitriani, S. Ikeda, M. Tani, H. Yajima, H. Furuta and A. Hatta, Hydrophilization of polytetrafluoroethylene using an atmospheric-pressure plasma of argon gas with water–ethanol vapor, Mater. Chem. Phys. **282**, 125974 (2022).

24. Y. Zhan, S. Yu, A. Amirfazli, A. R. Siddiqui and W. Li, Preparations of versatile polytetrafluoroethylene superhydrophobic surfaces using the femtosecond laser technology, Colloid. Surface. A. **629**, 127441 (2021).

25. S. F. Toosi, S. Moradi, S. Kamal and S. G. Hatzikiriakos, Superhydrophobic laser ablated PTFE substrates, Appl. Surf. Sci. **349**, 715–723 (2015).

26. L. Ferry, G. Vigier and J. L. Bessede, Effect of ultraviolet radiation on polytetrafluoroethylene: Morphology influence, Polym. Adv. Technol. **7**, 493-500 (1996).

27. Z. Qin, J. Ai, Q. Du, J. Liu and X. Zeng, Superhydrophobic polytetrafluoroethylene surfaces with accurately and continuously tunable water adhesion fabricated by picosecond laser direct ablation, Mater. Des. **173**, 107782 (2019).

28. S. Küper and M. Stuke, Ablation of polytetrafluoroethylene (Teflon) with femtosecond UV excimer laser pulses, Appl. Phys. Lett. **54**(1), 4 (1998).

29. M. Garcia-Lechuga and D. Grojo, Simple and robust method for determination of laser fluence thresholds for material modifications: an extension of Liu's approach to imperfect beams, Open. Res. Eur. **1**, 7 (2021).

30. V. Sirutkaitis, R. Jonušas, A. Bargelis, J. Kalpokas, K. Juzėnas, O. Balachninaitė, M. Peckus, V. Kudriašov and M. Barkauskas, *Lazerinių Technologijų Laboratoriniai Darbai*, (Vilniaus universitetas, 2008).

31. A. Bogaerts and Z. Chen, Effect of laser parameters on laser ablation and laser-induced plasma formation: A numerical modeling investigation, Spectrochim. Acta. B. **60**(9–10), 1280–1307 (2005).

32. S. Prakash and S. Kumar, Microchannel fabrication via direct laser writing, Microfab. Precis. Eng. 163–187 (2017).

33. S. Küper and M. Stuke, Ablation of UV-transparent materials with femtosecond UV excimer laser pulses, Microelectron. Eng. **9**(1–4), 475–480 (1989).

34. J. D. Bhawalkar, G. S. He and P. N. Prasad, Nonlinear multiphoton processes in organic and polymeric materials, Rep. Prog. Phys. **59**(9), 1041 (1996).

35. G. N., K. Kalli and K. Sugde, *Frontiers in Guided Wave Optics and Optoelectronics*, (Books on Demand, 2010).

36. S. M. Barinov, A. V. Kuznetsov, V. O. Kompanets, M. S. Komlenok, V. V. Kononenko, V. M. Gololobov and V. I. Konov, On the role of multiphoton absorption of light in pulsed laser nanoablation of diamond, Quantum. Electron+. **46**(2), 125 (2016).

37. M. Womack, M. Vendan and P. Molian, Femtosecond pulsed laser ablation and deposition of thin films of polytetrafluoroethylene, Appl. Surf. Sci. **221**(1–4), 99–109 (2004).

38. Y. Tian and L. Jiang, Intrinsically robust hydrophobicity, Nat. Mater. **12**(4), 291–292 (2013).

Summary

Mindaugas Česnulis

Wettability control of PTFE surfaces with femtosecond laser pulses

Material processing is an important field in industry allowing to cut, weld, drill, clean or modify any material physical property. Traditional techniques of material shaping rely on mechanical force and are not accurate regarding micro scale precision. Laser technology have emerged as superior approach to alter properties of different materials precisely. Surface modification is one of the easiest laser technology tool to apply on different materials – metals, polymers, semiconductors. Specifically, lasers producing femtosecond laser pulses makes it possible to affect transparent or hard materials, such as, diamond. Light-matter interaction span using such pulses is shorter than thermalization duration in atoms.[30] This feature allows us to make precise and clean ablation process without remelted zones, cracks, debris. Multifunctional surfaces exhibiting properties such as self-cleaning, anti-icing, corrosion and anti-biofouling on metals are widely applicable in everyday life.[19] Such properties can also be achieved for well-known solid polymers making them suitable materials for water repellent surfaces.[38]

The goal of this work was to investigate different laser fabrication parameters impact on PTFE surface wettability control. To achieve this, the surfaces of PTFE have been modified with two different laser radiation wavelengths by altering laser micromachining parameters, such as, pulses overlap (scanning velocity), number of rescans and distance between scanning lines. Besides flat textured surfaces, triangular profile pits have been made to achieve water confinement properties.

For PTFE material testing, by varying laser parameters ablated material depths of square pits were measured to be higher for higher number of rescans and lower periods. Quantitatively, hydrophobicity was determined by measuring water contact angle on all flat textured samples. It was found that highest CA was achieved using both 343 nm and 515 nm laser wavelengths and considered as superhydrophobic and equal to 171 degrees. The surface roughness parameter was measured on some specimens to identify its contribution to overall hydrophobicity. Higher scanning periods results in higher surface roughness values. Also, it was found that surface roughness significantly contributes to overall superhydrophobicity of PTFE surface as texture material CAs are more than 30 degrees higher than of bare material. Both second and third harmonic generations are capable to produce superhydrophobic surfaces, however, third harmonic generation is more time-effective solution.

Santrauka

Mindaugas Česnulis

Paviršiaus drėkinimo kontrolė PTFE medžiagoje femtosekundiniais lazerio impulsais

Medžiagų apdirbimas yra svarbi pramonės sritis leidžianti pjauti, virinti, gręžti, valyti ar modifikuoti bet kurią medžiagos fizinę savybę. Tradiciniai medžiagų manipuliavimo metodai, besiremiantys mechaninės jėgos panaudojimu, yra netikslūs siekiant mikro eilės tikslumo. Lazerinė technologija iškilo kaip pranašesnė už tradicinius medžiagos apdirbimo būdus norint tiksliai pakeisti skirtingų medžiagų savybes. Paviršiaus modifikavimas yra viena lengvesnių užduočių norint tai pritaikyti skirtingoms medžiagoms – metalams, polimerams, puslaidininkiams. Konkrečiai lazeriai generuojantys femtosekundinius impulsus leidžia paveikti skaidrias ar kietas medžiagas, pavyzdžiui, deimantą. Šviesos-medžiagos sąveikos trukmė veikiant tokiems impulsams yra trumpesnė nei termalizacijos trukmė atomuose.[30] Ši savybė leidžia pasiekti tikslų ir švarų medžiagų abliacijos procesą be persilydžiusių plotų, įtrūkimų, nešvarumų. Multifunkciniai paviršiai, demonstruojantys nusivalančias, neledėjančias, korozijai ir biologiniam užterštumui atsparias savybes ant metalų, yra plačiai pritaikomi kasdieniniame gyvenime.[19] Tokios savybės gali būti pasiektos gerai žinomuose kietuose polimeruose, paverčiant juos tinkamomis medžiagomis vandeniui atspariems paviršiams formuoti.[38]

Šio darbo tikslas buvo ištirti skirtingų lazerinio apdirbimo parametrų poveikį PTFE paviršių drėkinimo kontroliavimui. Tam pasiekti, PTFE medžiagos paviršiai buvo modifikuoti naudojant du skirtingus lazerio bangos ilgius keičiant mikro apdirbimo parametrus: impulsų persiklojimą (skanavimo greitį), perskanavimų skaičių ir atstumą tarp skanavimo linijų. Be tekstūruotų plokščių plotų, trikampio formos profilio įdubimai buvo suformuoti norint pasiekti vandens manipuliavimo norima kryptimi savybių.

PTFE medžiagos testavimui buvo išmatuotas lazeriu pašalintos medžiagos tūris ir apdirbamo ploto gylis, keičiant apdirbimo parametrus. Plotų gyliai buvo didesni esant didesniam skanavimų skaičiui ir mažesniems skanavimo periodams. Kiekybiškai drėkinimas buvo nustatytas matuojant vandens kontaktinį kampą ant visų bandinių. Buvo išsiaiškinta, kad didžiausias kontaktinis kampas pasiektas naudojant tiek 343 nm, tiek 515 nm bangų ilgius ir gali būti laikomas superhidrofobišku, lygus 171 laipsniams, tačiau UV spinduliuotė efektyvesnė laiko atžvilgiu. Paviršiaus šiurkštumas buvo išmatuotas siekiant išsiaiškinti jo įtaką paviršiaus hidrofobiškumui. Didesni skanavimo periodai sąlygoja didesnes šiurkštumo vertes. Paviršiaus šiurkštumas ryškiai prisideda prie bendro PTFE paviršių superhidrofobiškumo, nes tekstūruota medžiaga turi 30 laipsnių didesnius drėkinimo kampus nei neapdirbta medžiaga.